IEEE Photonics Journal
An IEEE Photonics Society Publication

Open Access

3D Gerchberg-Saxton Optical Correlation

Volume 10, Number 2, April 2018

Wen Chen

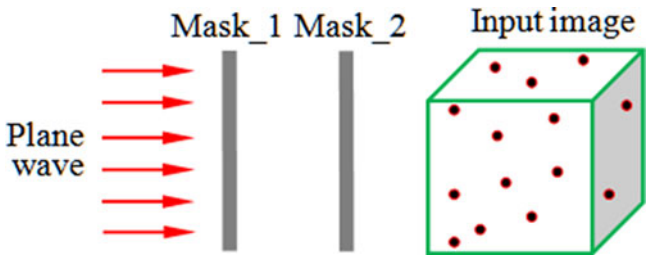

DOI: 10.1109/JPHOT.2018.2798602
1943-0655

IEEE photonics SOCIETY

IEEE

3D Gerchberg-Saxton Optical Correlation

Wen Chen

The Hong Kong Polytechnic University Shenzhen Research Institute, Shenzhen 518057, China, and Department of Electronic and Information Engineering, The Hong Kong Polytechnic University, Hong Kong, China

DOI:10.1109/JPHOT.2018.2798602

Manuscript received December 23, 2017; revised January 21, 2018; accepted January 23, 2018. Date of publication January 26, 2018; date of current version February 22, 2018. This work was supported in part by the National Natural Science Foundation of China (NSFC) under Grant 61605165, in part by Hong Kong Research Grants Council Early Career Scheme under Grant 25201416, in part by the Shenzhen Science and Technology Innovation Commission through Basic Research Program under Grant JCYJ20160531184426473, and in part by The Hong Kong Polytechnic University (4-BCDY, G-YBVU, 4-ZZHM, and 1-ZE5F). Corresponding author: W. Chen (e-mail: owen.chen@polyu.edu.hk).

Abstract: Since Gerchberg–Saxton algorithm was developed, it has been applied in various fields, e.g., optical display and optical tweezers. In this paper, three-dimensional (3D) Gerchberg–Saxton optical correlation is proposed. A 2D image is divided into particle-like points placed in 3D space, which are simultaneously encoded into the cascaded phase masks by using a modified Gerchberg–Saxton algorithm. The extracted phase masks can be flexibly compressed, and the decoded images can be verified via optical correlation. It is also illustrated that high security and high flexibility can be achieved by using the proposed 3D Gerchberg–Saxton correlation method. The proposed 3D Gerchberg–Saxton algorithm can provide a new and significant insight on optical correlation.

Index Terms: Optical processing, optical correlation, phase retrieval.

1. Introduction

Gerchberg-Saxton algorithm [1] has become an interesting phase retrieval method for various fields [2]–[5], such as optical display, light shaping and tweezers. However, conventional Gerchberg-Saxton algorithm [1] is limited by a *priori* knowledge about the test sample, and it is also concerned that the convergence rate is slow. Subsequently, a number of its derivatives [2]–[7], such as error reduction method, input-output method and oversampling, are continuously developed to resolve the problems.

The Gerchberg-Saxton algorithm has also been applied as one of the most useful techniques for the generation of phase-only holograms [8]. Since the generated hologram could be flexibly controlled by a device nowadays, optical approaches can be easily carried out. Due to this remarkable characteristic, Gerchberg-Saxton algorithm has also been further explored for optical security [9], [10]. An image can be encoded into phase patterns (or called computer-generated holograms) by using an iterative approach, and the decoding process can be conducted by using an optical or digital approach [9], [10]. However, conventional optical security approaches using Gerchberg-Saxton algorithm [9], [10] are limited to 2D space, and system security is constrained. Most established optical security systems [11]–[21] are focused on the development of encoding and decoding techniques, and optical authentication strategy [22] further provides an approach to establishing an

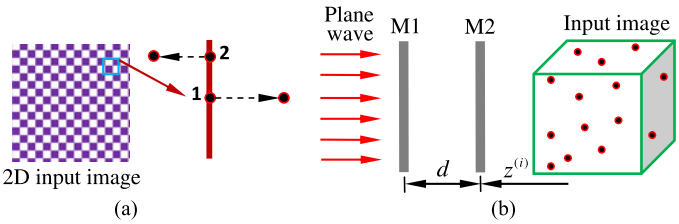

Fig. 1. (a) A schematic to illustrate the generation of particle-like points in 3D space [20], [23], [24], and (b) a schematic for 3D Gerchberg-Saxton correlation: M, phase mask which can be embedded into spatial light modulator in practice; d and z, axial distances. Integer i is 1, 2, 3, ..., P. For optical decoding, a CCD camera can be used to replace the input image plane, and is axially translated to record a series of intensity patterns.

additional security layer. However, conventional optical security systems using Gerchberg-Saxton algorithm do not use optical correlation in 3D space for security enhancement.

In this paper, 3D Gerchberg-Saxton optical correlation is proposed. A 2D image is divided into particle-like points placed in 3D space, which are simultaneously encoded into the cascaded phase-only masks by using a modified Gerchberg-Saxton algorithm. The extracted phase-only masks are flexibly compressed, and the decoded images can be verified via optical correlation. The results demonstrate that the security achieved in 3D Gerchberg-Saxton correlation approach is high, and high flexibility can also be achieved.

2. Principles

A schematic for 3D Gerchberg-Saxton correlation approach is illustrated in Fig. 1(a) and (b). The input image with 512×512 pixels is divided into a series of particle-like points, and neighboring pixels of the input image, such as 16×16 pixels, are combined and generated as a particle-like point [20], [23], [24] as illustrated in Fig. 1(a) and (b). The generated particle-like points are placed in different axial positions to establish a 3D space for the encoding.

For the sake of brevity, all particle-like points are encoded into only two cascaded phase-only masks M1 and M2, and it is straightforward to generate a different number of cascaded phase-only masks in practice. The encoding process is described as follows:

1) Initially, random patterns are generated, i.e., for M1 and M2. Here, $M_1^{(i,n)}(x, y)$ and $M_2^{(i,n)}(\xi, \eta)$ are used to respectively represent M1 and M2, where i denotes particle-like point index ($i = 1, 2, \ldots, P$), and n denotes iteration number ($n = 1, 2, \ldots, N$). At the initial iteration, i and n are set as 1. The propagation process between M1 and M2 can be illustrated as follows:

$$O(\xi, \eta) = \mathrm{FSP}_d\left[M_1^{(i,n)}(x, y)\right], \tag{1}$$

where d represents the distance, $O(\xi, \eta)$ denotes complex-valued wavefront just before phase-only mask M2, and FSP denotes free-space wave propagation [25].

2) Wave propagate forward to generate $O(\mu^{(i)}, \nu^{(i)})$ in a specific particle-like point (i.e., i) plane:

$$O(\mu^{(i)}, \nu^{(i)}) = \mathrm{FSP}_{z^{(i)}}\left[M_2^{(i,n)}(\xi, \eta) O(\xi, \eta)\right], \tag{2}$$

where $z^{(i)}$ denotes axial distance between the M2 plane and each particle-like point (i.e., i) plane.

3) In input image plane, support constraint is further used.

$$\hat{O}(\mu^{(i)}, \nu^{(i)}) = \mathrm{CS}\left[O(\mu^{(i)}, \nu^{(i)})\right], \tag{3}$$

where CS denotes the constraint given by [24]

$$\mathrm{CS}\left[O(\mu^{(i)}, v^{(i)})\right] = \begin{cases} \frac{\left[2\delta I(\mu,v) - \left|O(\mu^{(i)},v^{(i)})\right|\right] O(\mu^{(i)},v^{(i)})}{\left|O(\mu^{(i)},v^{(i)})\right|} & \text{if } (\mu, v) \in i \\ O(\mu^{(i)}, v^{(i)}) & \text{if } (\mu, v) \notin i \end{cases}, \tag{4}$$

where $I(\mu, \nu)$ is desired input image, $|\ |$ denotes modulus operation, and δ denotes a ratio between the summation of calculated output and the summation of the desired input image within a particle-like point (i.e., i). Since the 2D input image is divided into a series of particle-like points to be placed at different axial positions, each time only one particle-like point has to be updated as illustrated in (4).

4) Updating M2 and M1:

$$\hat{M}_2^{(i,n)}(\xi, \eta) = \left\{ \frac{\mathrm{FSP}_{-z^{(i)}}\left[\hat{O}\left(\mu^{(i)}, \nu^{(i)}\right)\right]}{\mathrm{FSP}_d\left[M_1^{(i,n)}(x, y)\right]} \right\} \Bigg/ \left| \frac{\mathrm{FSP}_{-z^{(i)}}\left[\hat{O}\left(\mu^{(i)}, \nu^{(i)}\right)\right]}{\mathrm{FSP}_d\left[M_1^{(i,n)}(x, y)\right]} \right|, \tag{5}$$

$$\hat{M}_1^{(i,n)}(x, y) = \frac{\mathrm{FSP}_{-d}\left(\left\{\mathrm{FSP}_{-z^{(i)}}\left[\hat{O}\left(\mu^{(i)}, \nu^{(i)}\right)\right]\right\}\left[\hat{M}_2^{(i,n)}(\xi, \eta)\right]^*\right)}{\left|\mathrm{FSP}_{-d}\left(\left\{\mathrm{FSP}_{-z^{(i)}}\left[\hat{O}\left(\mu^{(i)}, \nu^{(i)}\right)\right]\right\}\left[\hat{M}_2^{(i,n)}(\xi, \eta)\right]^*\right)\right|}, \tag{6}$$

where $\mathrm{FSP}_{-z^{(i)}}$ and FSP_{-d} denote back-propagation [25], and $\hat{M}_1^{(i,n)}(x, y)$ and $\hat{M}_2^{(i,n)}(\xi, \eta)$ are the updated M1 and M2, respectively.

All particle-like points are sequentially processed by using (1)–(6), and one iteration is completed only when all particle-like points are used for the update. After all particle-like points are processed, the updated M1 and M2 [i.e., $\hat{M}_1^{(P,n)}(x, y)$ and $\hat{M}_2^{(P,n)}(\xi, \eta)$] are further employed, i.e., replacing n by $n + 1$. Difference between amplitude maps of two neighboring 2D wavefronts in the input image plane is calculated, i.e., $\{\sum_{\mu,\nu}[|\hat{O}^{(n)}(\mu, \nu)| - |\hat{O}^{(n-1)}(\mu, \nu)|]^2\}/(512 \times 512)$,where $\hat{O}^{(n)}(\mu, \nu)$ denotes 2D complex-valued wavefront obtained by incorporating all particle-like points. After the difference is determined, a threshold is used to judge whether the iteration operation can be stopped. It is worth noting that when a new iteration starts, the particle-like point index i should be initialized as 1. The finally generated phase-only masks M1 and M2 are denoted as $M_1(x, y)$ and $M_2(\xi, \eta)$,respectively. To conduct the correlation without disclosure of input image, the generated phase-only masks can be flexibly compressed, and in this study only the generated phase-only mask M1 [i.e., $M_1(x, y)$] is further compressed to illustrate the proposed method. The compressed mask M1 is denoted as $\tilde{M}_1(x, y)$.

During the decoding, $\tilde{M}_1(x, y)$ and $M_2(\xi, \eta)$ are placed in the optical path, and can be embedded into phase-only spatial light modulators. In the proposed method, axial distances $z^{(i)}$ are applied as one of principal security keys. Every particle-like point can be sequentially decoded at a specific axial position, and then is determined by using the preset transverse region information. In practice, a CCD camera can be axially translated to record a series of images. Finally, the input image is decoded by incorporating all retrieved particle-like points in the transverse domain, and the decoded input image is denoted as $\hat{I}(\mu, \nu)$. The decoding process aforementioned could be described by

$$\hat{I}(\mu, \nu) = \underset{(\mu,\nu)}{\Im}\left(\underset{(\mu,\nu)}{\Re}\left|\mathrm{FSP}_{z^{(i)}}\left(\left\{\mathrm{FSP}_d\left[\tilde{M}_1(x, y)\right]\right\} M_2(\xi, \eta)\right)\right|^2\right), \tag{7}$$

where $\Re$ denotes a selection operation in the transverse domain, and $\Im$ denotes an incorporation operation in the transverse domain.

Since the decoded image does not render original information, a correlation is carried out for the verification. The correlation process is described by [22], [26]–[30]

$$C(\mu, \nu) = \left|\mathrm{IFT}\left(\left|[K(\xi, \eta)]\left[\hat{K}(\xi, \eta)\right]^*\right|^{\omega-1}[K(\xi, \eta)]\left[\hat{K}(\xi, \eta)\right]^*\right)\right|^2, \tag{8}$$

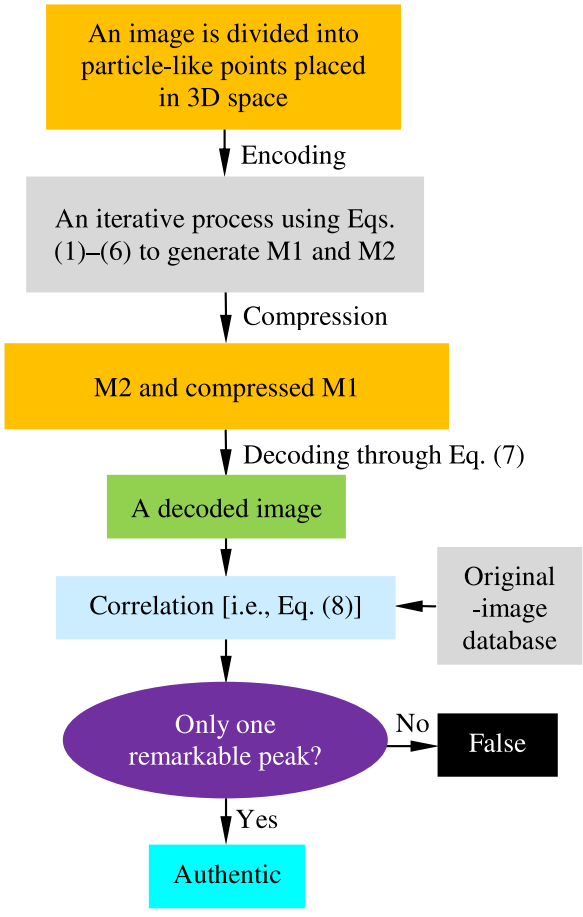

Fig. 2. Flow chart for illustrating 3D Gerchberg-Saxton optical correlation method. In practice, original-image database is invisible to the receiver, and only a platform interface is given.

where $K(\xi, \eta) = \mathrm{FT}[I(\mu, \nu)]$, $\hat{K}(\xi, \eta) = \mathrm{FT}[\hat{I}(\mu, \nu)]$, $C(\mu, \nu)$ denotes the generated correlation distribution, and ω is 0.30 in this study. Fig. 2 is further given to illustrate 3D Gerchberg-Saxton correlation approach.

3. Results and Discussion

The arrangement shown in Fig. 1(b) is numerically carried out to illustrate validity of 3D Gerchberg-Saxton correlation. The laser wavelength is 632.8 nm. A CCD with 4.65 μm and 512 $\times$ 512 pixels can be employed during the decoding. Axial distance d is 10.0 mm, and the series of axial distances $z^{(i)}$ is randomly distributed in a range of [5.0 mm, 20.0 mm]. Before the encoding, a grayscale input image ("Lena" with 8 bits and 512 $\times$ 512 pixels) is divided into particle-like points placed in 3D space as seen in Fig. 1(a) and (b). The 16 $\times$ 16 neighboring pixels of input image are generated as a particle-like point, hence 1024 particle-like points (i.e., $P = 1024$) are generated. In practice, it is straightforward to combine the smaller or bigger number of neighboring pixels as a particle-like point. In the proposed method, the encoding process is conducted to find M1 and M2 using several support constraints. In practice, the generated M1 and M2 can be displayed in spatial light modulators for the decoding. During optical decoding, when the series of axial positions is available, a CCD camera can be used and axially translated to sequentially record a series of patterns.

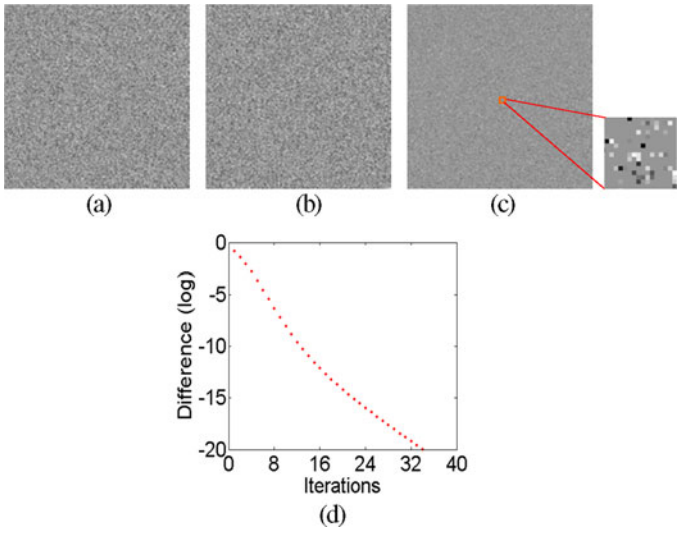

Fig. 3. (a) The extracted mask M1 [i.e., $M_1(x, y)$], (b) the extracted mask M2 [i.e., $M_2(\xi, \eta)$], (c) a compressed M1 [i.e., $\tilde{M}_1(x, y)$], and (d) a relationship between iteration number and the calculated differences (log scale).

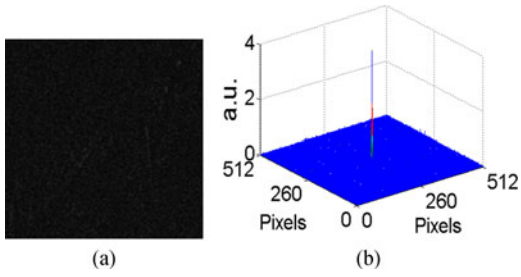

Fig. 4. (a) An image generated by using correct parameters, and (b) the generated correlation map for (a).

Fig. 3(a) shows the extracted mask M1 [i.e., $M_1(x, y)$], and Fig. 3(b) shows the extracted mask M2 [i.e., $M_2(\xi, \eta)$]. Since the correlation is conducted without observation of input image, the extracted masks can be compressed. Here, only M1 is compressed, and Fig. 3(c) shows a compressed phase mask M1 [i.e., $\tilde{M}_1(x, y)$]. Only 20.0% pixels of Fig. 3(a) are randomly selected and maintained, and others are set as zero. An inset has been given to clearly illustrate the compression operation applied to M1. A relationship between iteration number and the calculated differences is given in Fig. 3(d). A rapid convergence rate has been achieved. When all parameters are correct, a decoded image is shown in Fig. 4(a) and its corresponding correlation distribution is given in Fig. 4(b). The peak signal-to-noise ratio (PSNR) is 5.321 for Fig. 4(a). As seen in Fig. 4(a) and (b), original inputs cannot be visually observed, and there is only one peak. It is indicated that the receiver holds correct keys, or he/she is an authorized person.

Since 3D space is applied in the proposed method, the decoded image obtained at any section does not render sufficient information for correct correlation. Fig. 5(a), (c), and (e) show the decoded images, when only an axial distance, i.e., 5.0, 10.0 and 15.0 mm, is respectively applied between the M2 plane and CCD plane. The corresponding correlation maps are shown in Fig. 5(b), (d), and (f), respectively. It can be observed that noisy map is always produced. This indicates that the receiver is not an authorized person, or does not hold correct security keys. It is also demonstrated that the proposed 3D Gerchberg-Saxton correlation method possesses the higher security compared

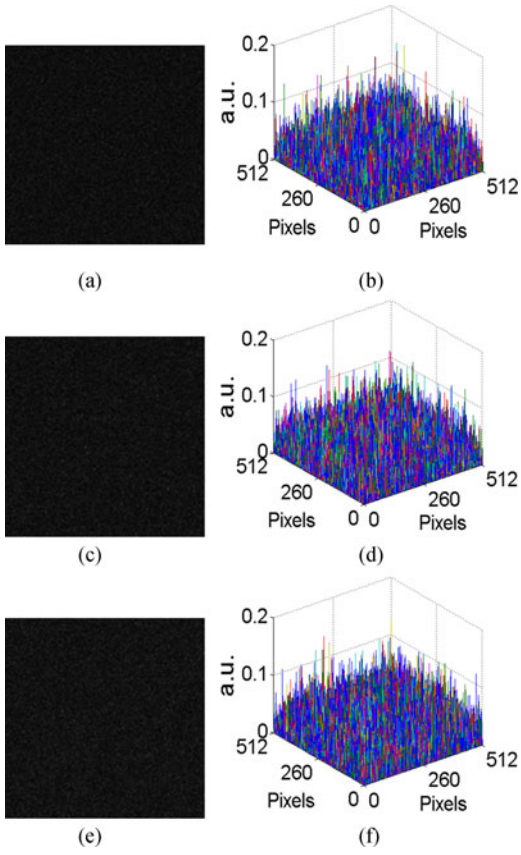

Fig. 5. The image generated when only (a) 5.0 mm, (c) 10.0 mm and (e) 15.0 mm is applied between the M2 plane and CCD plane. (b), (d) and (f) Correlation maps for (a), (c) and (e), respectively.

to previous works [26]. In the proposed method, when the number of sections (or correct axial positions) is closer to the number of generated particle-like points and transverse positions are assumed to be correct, correlation results of the decoded images can be closer to the pre-defined values.

In the proposed system, the series of axial distances $z^{(i)}$ is used as one of principal security keys. When it is incorrectly applied, a decoded image is given in Fig. 6(a) and its corresponding correlation distribution is illustrated in Fig. 6(b). Fig. 6(c) shows a decoded image, when the extracted mask M2 is wrong. Its correlation distribution is shown in Fig. 6(d). A noisy distribution is also generated.

The proposed method also provides high flexibility to modify compression ratio. When only 15.0% pixels of that in Fig. 3(a) are randomly selected and maintained (others are set as zero), a decoded image is given in Fig. 7(a) by using correct parameters. The PSNR value for Fig. 7(a) is 5.318. All other parameters are the same as those used for Fig. 4(a). The corresponding correlation distribution is shown in Fig. 7(b). When only 25.0% pixels of that in Fig. 3(a) are selected randomly, a decoded image is shown in Fig. 7(c). The PSNR value for Fig. 7(c) is 5.324. The corresponding correlation map is shown in Fig. 7(d). It is illustrated again that input image cannot be visually observed, but the decoded images can be effectively verified.

Discrimination capability of the proposed 3D Gerchberg-Saxton correlation method is further analyzed. When another input image (i.e., "Baboon" with 8 bits and 512×512 pixels) is encrypted and parameters used for Fig. 7(a) are also applied, Fig. 8(a) shows a decoded image using correct parameters. Fig. 8(b) shows a correlation map calculated between that in Fig. 8(a) and original image ("Lena"). Original images could be managed via a database which is not visible to the receiver,

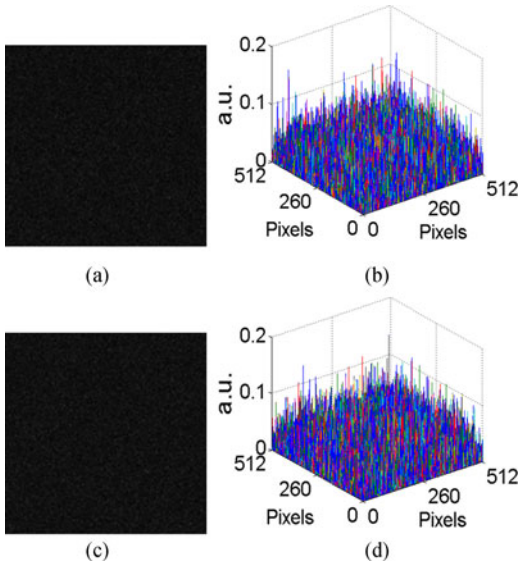

Fig. 6. (a) A decoded image obtained when the series of axial distances is incorrectly used, (b) the generated correlation map for (a). (c) A decoded image obtained when only M2 is wrong, (d) the generated correlation map for (c).

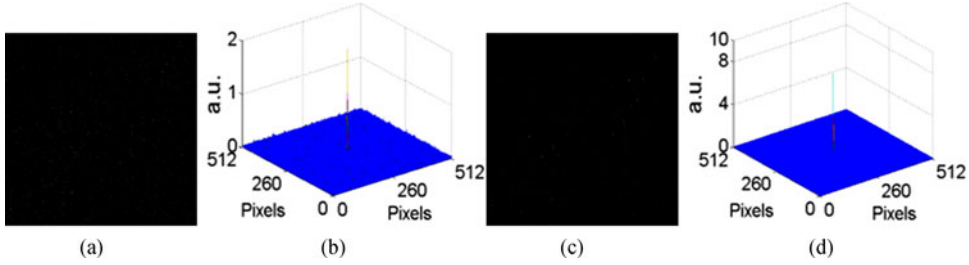

Fig. 7. (a) An image obtained using correct parameters when only 15.0% pixels of that in Fig. 3(a) are maintained and others are set as zero, (b) the generated correlation map for (a). (c) An image obtained using correct parameters when only 25.0% pixels of that in Fig. 3(a) are maintained and others are set as zero, (d) the generated correlation map for (c).

and only a platform interface is given [27]. When one more input image (i.e., "Cameraman" with 8 bits and 512 $\times$ 512 pixels) is encrypted and parameters used for Fig. 7(a) are also applied, Fig. 8(c) shows a decoded image obtained by using correct parameters. Fig. 8(d) shows a correlation map calculated between that in Fig. 8(c) and original image ("Lena"). It is observed that noisy correlation maps are generated, and the proposed method possesses high discrimination capability. Many other input images are also studied, and noisy correlation distributions are always generated. When the input image to be tested is similar to original image, we might further pre-define the parameters in the targeted or accurate correlation distributions, such as peak values, peak-to-background ratios, or even peak positions.

The proposed method possesses high flexibility to generate a large key space. For instance, various transform domains and different encoding structures can be applied. The phase mask M2 in Fig. 1(b) could also be applied as one of principal security keys. It is suggested that different series of axial positions can be used to encode different input images. In addition, original images can be stored in a separate database, which should be used for optical correlation. It can also be designed that the interface to database is only available to authorized persons. Hence, the proposed method with proper strategies can fully withstand potential attacks.

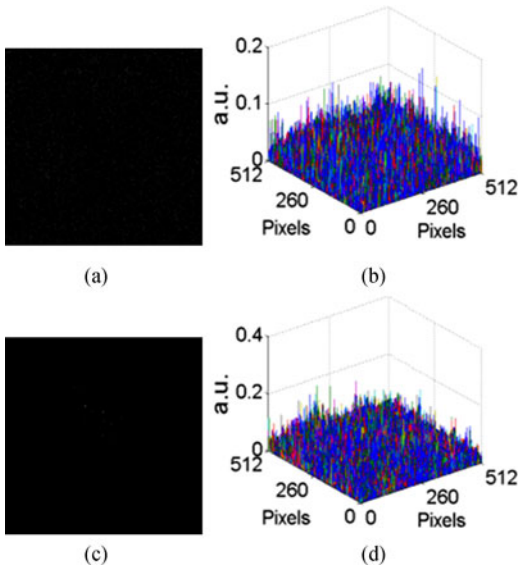

Fig. 8. Discrimination capability analysis: (a) A decoded image obtained by using correct parameters when another different image is encoded, (b) a correlation distribution calculated between that in (a) and original image. (c) A decoded image obtained by using correct parameters when one more different image is encoded, (d) a correlation distribution calculated between that in (c) and original image.

4. Conclusion

The 3D Gerchberg-Saxton optical correlation method has been proposed in this paper. A 2D image is divided into particle-like points placed in 3D space, which are simultaneously encoded into phase masks. A phase retrieval algorithm has been successfully developed and applied for the encoding in 3D space. A digital approach should be applied for the encoding, and there is a great potential to apply an optical way for the proposed decoding and correlation operations compared to previous works in 3D space. The computational results demonstrate that convergence rate is rapid in the proposed 3D Gerchberg-Saxton algorithm. The results also illustrate that the decoded images can be effectively verified, and high-security correlation is successfully implemented due to 3D space. In addition, high flexibility can also be achieved. The proposed 3D Gerchberg-Saxton algorithm can provide a new and significant insight on optical correlation.

References

[1] R. W. Gerchberg and W. O. Saxton, "A practical algorithm for the determination of phase from image and diffraction plane pictures," *Optik*, vol. 35, pp. 237–246, 1972.
[2] G. Whyte and J. Courtial, "Experimental demonstration of holographic three-dimensional light shaping using a Gerchberg-Saxton algorithm," *New J. Phys.*, vol. 7, 2005, Art. no. 117.
[3] S. P. Poland, N. Krstajić, R. D. Knight, R. K. Henderson, and S. M. Ameer-Beg, "Development of a doubly weighted Gerchberg-Saxton algorithm for use in multibeam imaging applications," *Opt. Lett.*, vol. 39, pp. 2431–2434, 2014.
[4] Y. Xu, Z. Ren, K. K. Y. Wong, and K. Tsia, "Overcoming the limitation of phase retrieval using Gerchberg-Saxton-like algorithm in optical fiber time-stretch systems," *Opt. Lett.*, vol. 40, pp. 3595–3598, 2015.
[5] J. Miao, P. Charalambous, J. Kirz, and D. Sayre, "Extending the methodology of X-ray crystallography to allow imaging of micrometer-sized non-crystalline specimens," *Nature*, vol. 400, pp. 342–344, 1999.
[6] J. R. Fienup, "Phase retrieval algorithms: A comparison," *Appl. Opt.*, vol. 21, pp. 2758–2769, 1982.
[7] J. R. Fienup and C. C. Wackerman, "Phase-retrieval stagnation problems and solutions," *J. Opt. Soc. Amer. A*, vol. 3, pp. 1897–1907, 1986.
[8] A. W. Lohmann and D. P. Paris, "Binary Fraunhofer holograms, generated by computer," *Appl. Opt.*, vol. 6, pp. 1739–1748, 1967.
[9] R. K. Wang, I. A. Watson, and C. Chatwin, "Random phase encoding for optical security," *Opt. Eng.*, vol. 35, pp. 2464–2469, 1996.

[10] E. G. Johnson and J. D. Brasher, "Phase encryption of biometrics in diffractive optical elements," *Opt. Lett.*, vol. 21, pp. 1271–1273, 1996.
[11] P. Refregier and B. Javidi, "Optical image encryption based on input plane and Fourier plane random encoding," *Opt. Lett.*, vol. 20, pp. 767–769, 1995.
[12] O. Matoba, T. Nomura, E. P. Cabré, M. S. Millán, and B. Javidi, "Optical techniques for information security," *Proc. IEEE*, vol. 97, no. 6, pp. 1128–1148, Jun. 2009.
[13] Y. Shi, T. Li, Y. Wang, Q. Gao, S. Zhang, and H. Li, "Optical image encryption via ptychography," *Opt. Lett.*, vol. 38, pp. 1425–1427, 2013.
[14] W. Chen, X. Chen, and Colin J. R. Sheppard, "Optical image encryption based on diffractive imaging," *Opt. Lett.*, vol. 35, pp. 3817–3819, 2010.
[15] T. J. Naughton, B. M. Hennelly, and T. Dowling, "Introducing secure modes of operation for optical encryption," *J. Opt. Soc. Amer. A*, vol. 25, pp. 2608–2617, 2008.
[16] X. F. Meng *et al.*, "Two-step phase-shifting interferometry and its application in image encryption," *Opt. Lett.*, vol. 31, pp. 1414–1416, 2006.
[17] L. Chen and D. Zhao, "Optical color image encryption by wavelength multiplexing and lensless Fresnel transform holograms," *Opt. Exp.*, vol. 14, pp. 8552–8560, 2006.
[18] A. Alfalou, C. Brosseau, N. Abdallah, and M. Jridi, "Simultaneous fusion, compression, and encryption of multiple images," *Opt. Exp.*, vol. 19, pp. 24023–24029, 2011.
[19] G. Situ and J. Zhang, "Position multiplexing for multiple-image encryption," *J. Opt. A, Pure Appl. Opt.*, vol. 8, pp. 391–397, 2006.
[20] W. Chen and X. Chen, "Space-based optical image encryption," *Opt. Exp.*, vol. 18, pp. 27095–27104, 2010.
[21] X. Wang, D. Zhao, F. Jing, and X. Wei, "Information synthesis (complex amplitude addition and subtraction) and encryption with digital holography and virtual optics," *Opt. Exp.*, vol. 14, pp. 1476–1486, 2006.
[22] E. Pérez-Cabré, M. Cho, and B. Javidi, "Information authentication using photon-counting double-random-phase encrypted images," *Opt. Lett.*, vol. 36, pp. 22–24, 2011.
[23] W. Chen, "Optical multiple-image encryption using three-dimensional space," *IEEE Photon. J.*, vol. 8, no. 2, Apr. 2016, Art. no. 6900608.
[24] W. Chen, X. Chen, and Colin J. R. Sheppard, "Optical image encryption based on phase retrieval combined with three-dimensional particle-like distribution," *J. Opt.*, vol. 14, 2012, Art. no. 075402.
[25] J. W. Goodman, *Introduction to Fourier Optics*, 2nd ed. New York, NY, USA: McGraw-Hill, 1996.
[26] W. Chen, B. Javidi, and X. Chen, "Advances in optical security systems," *Adv. Opt. Photon.*, vol. 6, pp. 120–155, 2014.
[27] W. Chen and X. Chen, "Grayscale object authentication based on ghost imaging using binary signals," *EPL*, vol. 110, 2015, Art. no. 44002.
[28] D. Fan *et al.*, "Multiple-image authentication with a cascaded multilevel architecture based on amplitude field random sampling and phase information multiplexing," *Appl. Opt.*, vol. 54, pp. 3204–3215, 2015.
[29] J. Chen, N. Bao, and Z. Zhu, "Optical information authentication via compressed sensing and double random phase encoding," *J. Opt.*, vol. 19, 2017, Art. no. 105702.
[30] W. Chen, X. Chen, A. Stern, and B. Javidi, "Phase-modulated optical system with sparse representation for information encoding and authentication," *IEEE Photon. J.*, vol. 5, no. 2, Apr. 2013, Art. no. 6900113.